Design boundaries of large-scale falling particle receivers

Jin-Soo Kim, Apurv Kumar, and Clotilde Corsi

Citation: AIP Conference Proceedings **1850**, 030029 (2017); doi: 10.1063/1.4984372
View online: http://dx.doi.org/10.1063/1.4984372
View Table of Contents: http://aip.scitation.org/toc/apc/1850/1
Published by the American Institute of Physics

Design Boundaries of Large-Scale Falling Particle Receivers

Jin-Soo Kim[1, a)], Apurv Kumar[2], Clotilde Corsi[1]

[1]*CSIRO Energy, PO Box 330, Newcastle, NSW 2300, Australia,*
[2]*Research School of Engineering, Australian National University, Canberra, Australia*
[a)]Corresponding author: jin-soo.kim@csiro.au

Abstract. A free falling particle receiver has been studied to investigate the design boundary of large-scale falling particle receivers. Preliminary receiver geometry and condition of falling particle curtain were scoped according to the nominal receiver capacity (135 MW_{th}), receiver outlet temperature (800 ^{o}C) and temperature difference (147 ^{o}C) recommended by the research program. Particle volume fraction and solar energy absorptivity were analyzed for two particle sizes (280 μm and 697 μm) in different flow range. The results were then converted to part load efficiency of the receiver. Ray tracing with a scoped receiver design provided the amount of spillage and overall performance of the receiver which comprises multiple cavities with different solar energy inputs. The study revealed and quantified some inherent problems in designing falling particle receivers such as, transmission energy loss caused by low solar energy absorption, efficiency decrease in part load operation, and uneven temperature distribution across falling particle curtain.

INTRODUCTION

Particle receiver is generating increased attention for its potential applicability in concentrated solar power (CSP) system[1-3]. Using solid particles as heat absorption and heat transfer media while avoiding complex receiver design makes the technology attractive. In addition, the particles provide cost effective thermal storage capability exceeding the temperature limit of the current thermal storage technology, which is essential to enable higher efficiency power blocks (like supercritical CO_2 Brayton system) to be integrated into CSP systems. ASTRI (Australia Solar Thermal Research Initiative) has identified the particle receiver technology as one of the promising options for achieving a high-efficiency and low-cost receiver. It is expected that the new designs will significantly reduce overall electricity generation cost in conjunction with other novel components of the CSP system. As a part of the ASTRI receiver development activity, CSIRO has been focusing on the falling particle receiver technology to develop novel concepts and apply them for designing commercial-scale systems for ASTRI's interest.

The objective of this study is to provide high-level information on the design boundaries of large-scale falling particle receivers. The study uses the simple free falling concept and investigated heat transfer characteristics and receiver performance for different design parameters. The outcome of the study provides various design aspects including receiver geometry, flow rate, particle discharge aperture size, particle velocity, particle volume fraction, particle temperature distribution, heat loss and receiver performance.

MODELLING CONDITION AND METHODOLOGY

Nominal power generation of 25 MW_e and solar multiple of 2.5 were considered for the preliminary design capacity of a reference CSP plant. Receiver capacity corresponding to the reference plant was estimated to be 135 MW_{th} considering initial assumption on power block and receiver efficiencies. Targeted particle outlet temperature is 800 °C with 147 °C increase from inlet temperature. The design capacity and operating condition (Table 1) are as per ASTRI goals considering supercritical carbon dioxide (SCO_2) Brayton cycle as a power block which are expected to evolve. Properties of particles (Table 2) were assumed to be same with those of CARBO Accucast which was used for particle receiver research by Ho et.al.[1]

SolarPACES 2016
AIP Conf. Proc. 1850, 030029-1–030029-8; doi: 10.1063/1.4984372
Published by AIP Publishing. 978-0-7354-1522-5/$30.00

TABLE 1. Preliminary design condition of the receiver.

System capacity, MW_e	25	capacity of ASTRI reference system
Solar multiple (SM)	2.5	suggested by ASTRI to meet 4 hours storage
Net power ratio	0.9	assuming 10 % parasitic consumption
Power block efficiency	0.515	suggested by ASTRI considering SCO_2 Brayton
Receiver capacity, MW_{th}	135	(system capacity • solar multiple) / (power block efficiency • net power ratio)
Receiver outlet temperature, ^oC	800	goal of ASTRI particle receiver
Receiver temperature increase, ^oC	147	suggested by ASTRI considering SCO_2 Brayton

TABLE 2. Particle properties[1] used for the study

Mass flow rate	2.79, 7, 15, 30 kg/s-m
Particle diameter	280 and 697 μm
Packed particle reflectivity	0.09
Heat capacity, C_p	$365T^{0.18}$ J/kg K
Particle density	3,300 kg/m^3

Modelling of the particle receiver comprises 1) simulating hydrodynamics to obtain local volume fractions of falling particles, 2) calculating the amount of solar energy attenuated by particles and 3) estimating receiver performance through energy balance and heat transfer calculations.

Investigation of falling particle hydrodynamics can be carried out either by a simple analytical model (assuming a no drag falling) or by using a CFD (ANSYS FLUENT) analysis. In order to reduce CFD computational time, an Eulerian-Eulerian multiphase model was used in this study. The result of CFD analysis was then used to calculate attenuated solar energy by each discretized volume of the falling particle curtain with the help of a Monte Carlo (MC) ray tracing simulation[3]. Finally, energy balance over discretized volumes of falling particle curtain gives temperature distribution of falling particles and the overall receiver performance. For increased accuracy, the MC ray tracing can be coupled with the CFD solver to update the temperature dependent properties in the computational model. However, present study is decoupled and the results do not update the temperature dependent properties in the CFD simulation. Hence, the results are recommended to be used only as an initial reference for scoping the design boundary of the free falling particle receiver.

DESIGN BOUNDARY OF FREE FALLING PARTICLE RECEIVERS

Receiver Geometry and Particle Flow Rate

Estimating the flow rate of falling particles per unit width of particle curtain is an important design factor of a falling particle receiver. Total particle flow rate is determined by the receiver capacity, particle heat capacity and particle temperature increase. Total area of falling particle curtain is related to the flux of solar irradiance and heat loss. Particle flow rate per falling width (kg/s-m) can be estimated by these two factors and the geometry of the receiver. If three basic geometries, square billboard and two cylinders with different diameter-height ratios are assumed as shown in Figure 1, the particle flow rate per width and the falling height can be estimated to scope the receiver dimension and falling condition. Comparison of the results for different conditions are provided in Figure 2. The figure reveals that flow rate per width increases when 1) particle heat capacity decreases, 2) solar flux increases, and 3) the aspect ratio of expanded receiver surface becomes square. In this study, case 3 geometry with around 6 m falling height and up to 30 kg/s-m flow rate were chosen as for initial design study.

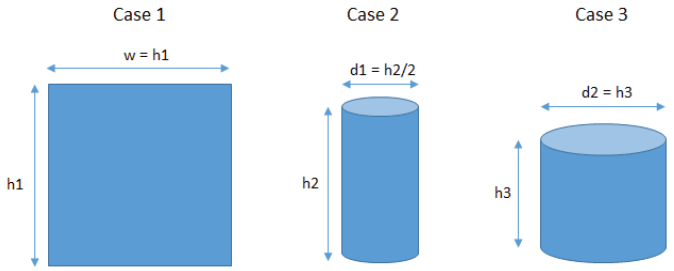

FIGURE 1. Three basic geometries of receiver surface; case 1: square billboard, case 2: long cylinder, case 3: short cylinder (cylinder type falling can be divided and reconfigured for multiple receivers).

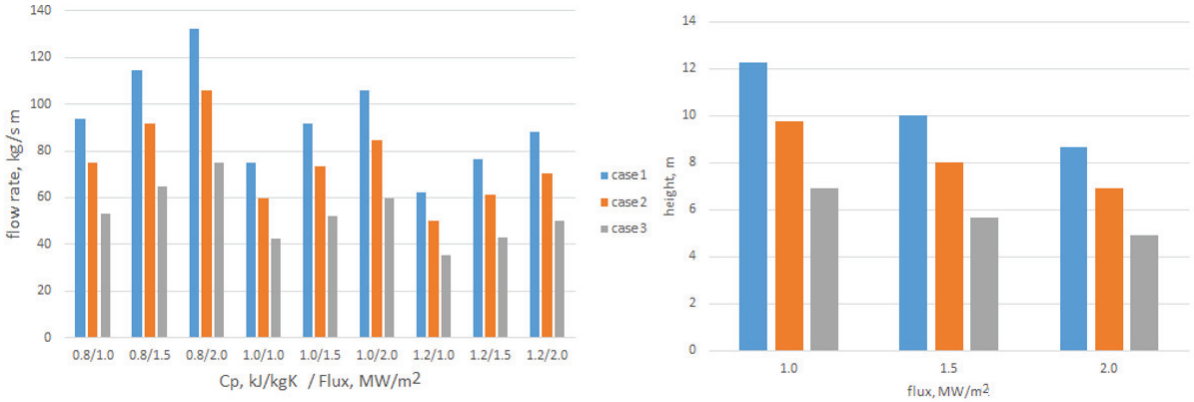

FIGURE 2. Flow rate per width of particle curtain (left) and falling height (right) for different design conditions.

Particle Discharge Aperture Size and Initial Velocity

Accurate size (width) of particle discharge aperture of the top hopper corresponding to desired flow rate is an important factor. In this study, a series of CFD simulations established correlation between the flow rate and aperture size for different particle sizes. The results were also validated with experimental data in our previous study[3]. Using the correlation between particle discharge aperture size and flow rate for different particle sizes, initial falling velocity for different analysis conditions were determined and used for the studies.

Figure 3 shows particle discharge aperture width, initial falling velocity, and initial particle volume fraction for four different flow rates and two different particle sizes. The range of the flow rate is to cover from full-scale design condition of this study to about 10 % part load operating condition. The results show that smaller particle requires slightly smaller aperture width but it creates notable difference in initial falling velocity and particle volume fraction.

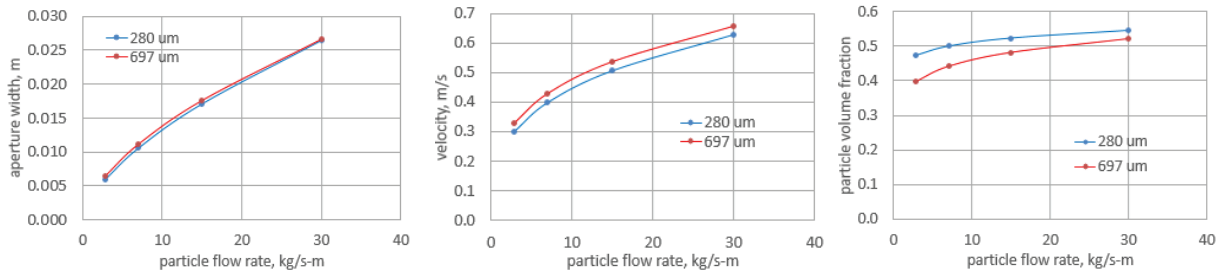

FIGURE 3. Particle discharge aperture width (left) and initial falling velocity (middle) and initial particle volume fraction (right) simulated by CFD at various particle flow rate.

Particle Falling Velocity and Volume Fraction

Once the initial falling velocity and particle volume fraction are obtained by CFD, velocity and volume fraction changes during the falling can be reasonably estimated by assuming an accelerated free falling without drag. Clustered particle falling is known to mimic no drag falling regardless of particle size[1, 4].

Figure 4 shows particle falling velocity and volume fraction changes during no drag falling of particles in full-scale height. Once particles start falling, the volume fraction of particles decreases very rapidly due to accelerated falling velocity and the time difference in falling between particles. Significant volume fraction change occurs during the initial 1 m falling. Volume fraction of particles increases as the flow rate increases. Larger particle size shows slightly higher volume fraction than that of smaller particle size. This is because initial falling velocity of larger particle is slightly higher than the smaller one (as shown in Figure 3).

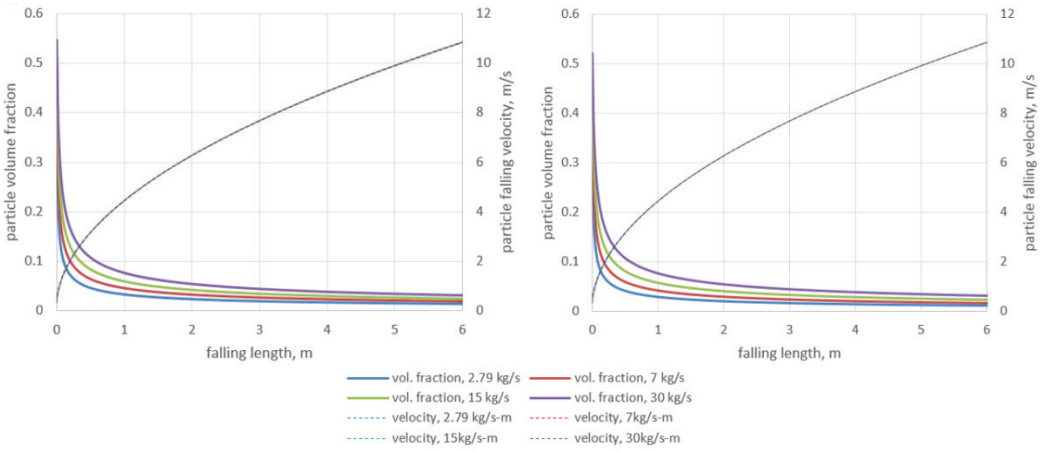

FIGURE 4. Volume fraction change during no drag falling of particles (left: 280 μm, right: 697 μm).

Absorption and Transmission of Solar Energy

Radiated solar energy into the particle curtain is either absorbed by particles, reflected to environment, or transmitted through the particle curtain. For a given reflectivity of the particle, the amount of absorbed energy by the particle curtain increases by increasing the volume fraction of particles and by decreasing the particle size. If an insulation material is considered for the wall behind the particles, most of transmitted solar energy is reflected back and is either absorbed by particles or transmitted out of the receiver and is finally lost. The energy loss by the transmission can be a matter of concern especially in the lower section of the receiver when operated under part load condition. Solar energy absorbed by the particle curtain at different falling length was obtained by calculating attenuated solar radiation through MC method[3] using the volume fraction.

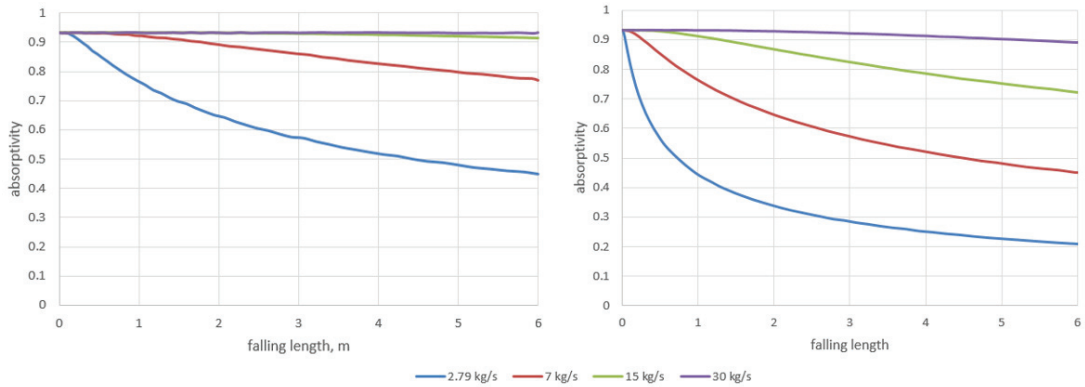

FIGURE 5. Absorptivity of solar energy by 6 m high free falling particle receiver for different flow rates and particle sizes.

The absorptivity of particle curtain is shown in Figure 5. The absorptivity is the fraction of overall energy absorbed by particles in both directions of solar ray travel (before and after reflection at the wall behind particle curtain). Accordingly, 1–absorptivity indicates total fraction of energy loss by both direct reflection (at the particle surface) and transmission. For a given particle size, the highest absorptivity is given by the highest volume fraction. As expected, the absorptivity decreases as flow rate decreases and as falling height increases. It is to be noted that the absorptivity decreases significantly as particle size increases even though the volume fractions are similar each other. Low absorptivity due to low flow rate or long falling height is an inherent problem of falling particle receiver as particle flow is directly exposed to solar radiation. Such a problem does not occur in typical tubular receivers because the pipe wall is completely opaque. To minimize this problem, choosing a smaller particle size is an option to take. But the problem still exists at the lower section of the receiver in part load operation. If the receiver is designed to create higher temperature difference than the case of this study, the design flow rate will get smaller for the same receiver capacity, which will increase the transmitted energy loss problem

Overall absorptivity for the entire length of falling for different flow rates and particle sizes are shown in Figure 6. The figure shows how much negative effect on the absorptivity is created by flow rate reduction (i.e. part load operation) for the 6 m falling case. As indicated by the detailed absorptivity results, smaller particle size provides much higher overall absorptivity in reduced flow rate conditions.

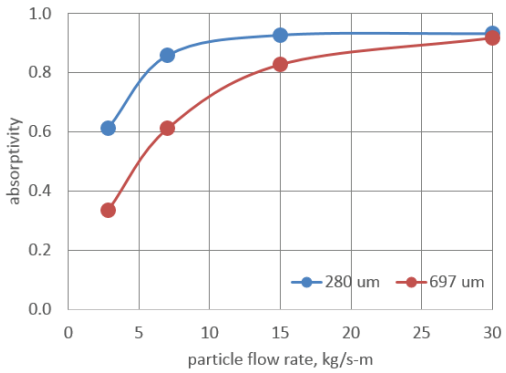

FIGURE 6. Overall absorptivity of 6 m falling particle receiver in different particle flow rates.

Temperature Distribution

Temperature distribution across the particle curtain is another interesting aspect to be investigated. Since the free falling particles are not likely to be vigorously mixed, unevenly absorbed solar energy across the particle curtain may cause local damage to particles thus limiting the operating condition. The MC model with multi-segment across the particle curtain and particle hydrodynamics simulated by CFD were used to obtain the temperature variation across the particle curtain[3]. The results (from a case of 500 K particles receiving 1 MW/m^2 solar irradiance) are plotted in Figure 7 at distance 1 and 1.5 m from the top of the receiver. These temperatures are only indicative and are to be used only as a first approximation since emission and convection losses are not considered in energy balance.

The figure shows that there are significant difference (400 ~ 500 K) between the highest (at front) and lowest (at rear) temperatures in the particle curtain for all flowrates. In addition, the shape of distribution is different for higher and smaller flowrate. Lower flowrate shows a “L” shape with two zones (front and rear) clearly distinguishable. While higher flowrates have a “Z” shape with a transition between the front and rear segments. Kumar et al.[3] also indicated that larger particle also shows similar temperature distribution pattern but smaller temperature difference between front and rear particles. Z shape of the temperature distribution is because of increased volume fraction and wider falling curtain. A large portion of the solar radiation is absorbed in the core of the curtain where the mass-flowrate of the particles is the highest, which restrict further-penetration of solar energy.

Though the temperature approximation was based only on absorbed energy, the likelihood of this non-uniform temperature distribution will increase the risk of particle material failure as well as failure of any other surface they come in contact with, such as receiver wall, or the particle heat exchanger surface.

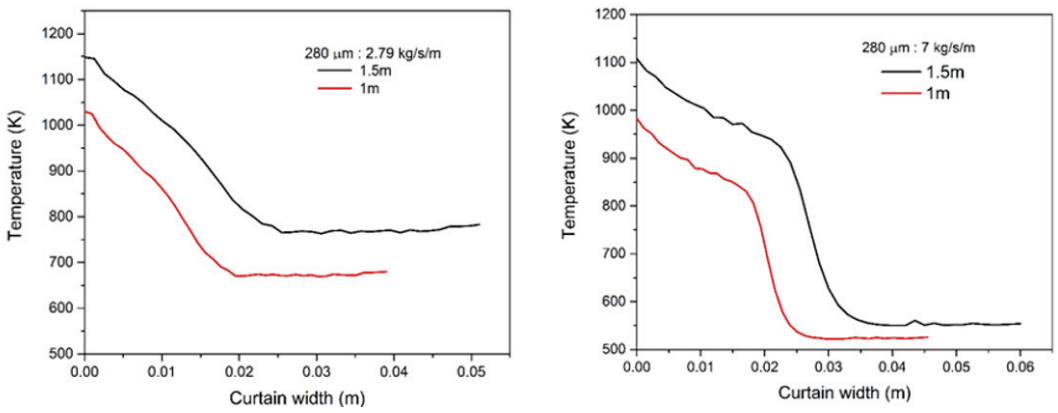

FIGURE 7. Temperature distribution across the curtain width at 1.5 m and 1 m from top for 280 μm particle[3] (width = 0 denotes front of the curtain facing the radiation).

Part Load Efficiency

By combining the absorptivity results (shown in Figure 6) and other relevant heat losses, efficiency of falling particle receiver can be estimated. A quick estimation of high-level receiver efficiency was carried out by considering simple assumptions for different heat losses as follows.

- Receiver dimension (as described in Table 3 and illustrated in Figure 9).
- Reflection & transmission energy loss: as per the absorptivity shown in Figure 6 and multiplied by an assumed ratio (0.63 in this study) of aperture area to receiver surface area of a cavity receiver.
- Emission heat loss: emission to ambient from an aperture size surface with 0.85 effective emissivity and 800 ^{o}C temperature.
- Convection heat loss: assumed to be 50 % of emission heat loss.

TABLE 3. Preliminary receiver configuration and dimension.

Type: multiple cavity (for ASTRI reference solar field)
Number of cavities: 4
Diameter of each cavity aperture: 6 m
Number of falling particle curtain per cavity: 3
Width of falling particle curtain: 2.5 m
Effective height of falling particle curtain: 6 m

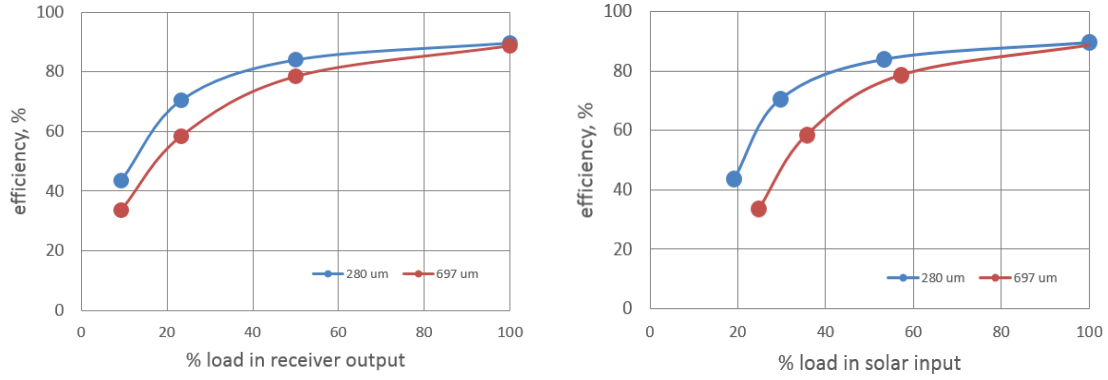

FIGURE 8. Estimated receiver efficiency again % load in receiver output power (left) and % load in solar input to receiver (right).

Given the assumptions, estimated receiver efficiency in different part load conditions are plotted in Figure 8. The definition of part load can be based on either receiver output power (Figure 8, left) or solar energy input (Figure 8, right). 100 % load condition was defined by 30 kg/s-m (in receiver flow rate) and 44 MW (in total solar energy provided through aperture) in the figure. Part load in solar input corresponds to more serious part load condition in receiver output because of increased heat loss when the receiver runs in part load. For all efficiency calculations, spillage were not taken into account.

Under the full load design condition, the receiver performance was 89.6 % and 88.8 % for 280 μm and 697 μm particle sizes, respectively. Under part load receiver operations with fixed inlet and outlet temperatures, efficiency decreases as the percentage load decreases. For a particle receiver, the efficiency decrease in part load operation is further enhanced by transmitted solar energy which increases as the flow rate decreases and as the particle size increases. For a highly-efficient particle receiver, high transmission of solar energy across the particle curtain (especially in part load operation) needs to be avoided.

RECEIVER CONCEPT AND HIGH-LEVEL PERFORMANCE

Basic receiver concept and high-level performance were investigated considering ASTRI reference plant. Preliminary configuration of solar field was given by ASTRI through an optimization for a typical cylindrical central receiver system located in Alice Springs, Australia. The scoped receiver concept for this solar field consists of 4 cavities dedicated for four 90 degree sections of the field. Solar field and receiver configurations are shown in Figure 9.

The amount of solar energy provided through each cavity aperture was calculated for different times of year using a ray tracing software[5]. Result of the ray tracing simulation are provided in Table 4 along with the amount of spilt energy. Total energy provided in equinox is 143.3 MW. This value is slightly smaller than the intended design value when energy loss is considered. The amount of spilt energy ranged 6.6 to 11.3 % but the level of spillage is expected to be reduced by further customizing the solar field suitable for the multiple cavity receiver concept.

Based on the same assumptions for a high-level performance estimation stated in previous section, overall receiver efficiency (considering all 4 cavities) at equinox (deemed as a design condition) is about 88 % (for 280 μm particle size). Slight decrease from the full load efficiency (89.6 %) is because of multiple cavities with different solar input comprising one receiver.

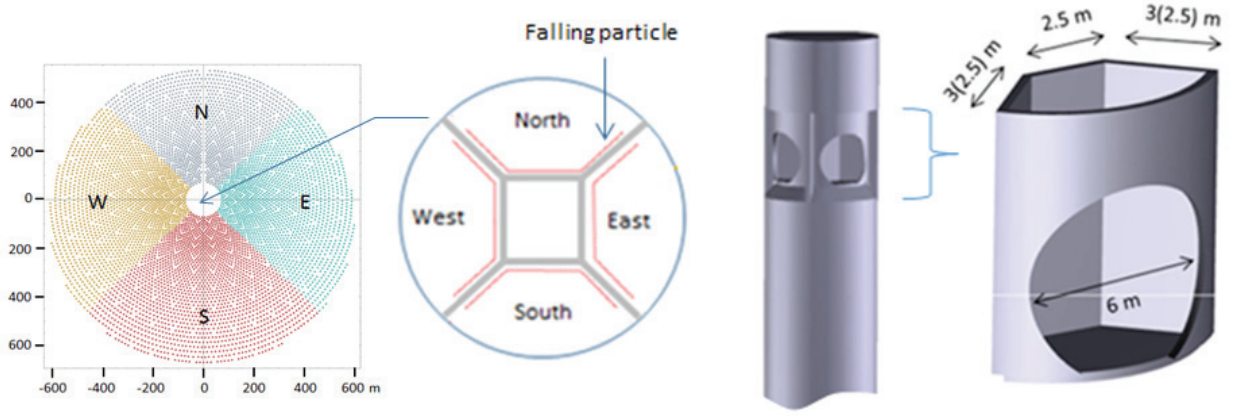

FIGURE 9, Concept geometry of a receiver employing 4 cavities compatible with the ASTRI reference field optimized for a system in Alice Springs, Australia, (assumed heliostat size: 6.1 m x 6.1 m, number of heliostats: 6,177, tower height: 92 m).

TABLE 4. Spillage and solar energy provision through aperture (time: solar noon).

	spillage, %			energy through aperture, MW		
	summer solstice	equinox	winter solstice	summer solstice	equinox	winter solstice
East	8.6	8.8	9.0	36.1	35.6	34.0
West	8.9	9.1	9.6	36.7	36.2	34.5
South	11.3	10.9	11.1	40.2	44.8	47.4
North	6.6	8.0	11.2	31.8	26.8	20.4
total				144.9	143.3	136.4

CONCLUSIONS

Design boundary of a large-scale falling particle receiver was investigated through hydrodynamics simulation of falling particle curtain, analysis on solar energy absorption characteristics, heat transfer, ray tracing and thermal performance estimation. Outcome of the study can be outlined as follows:

- Particle falling condition (such as flow rate per width of falling curtain, falling height and volume fraction change and etc.) varies depending on the intensity of solar energy irradiance, receiver geometry and particle properties and size.
- Solar energy absorption by falling particle increases as particle volume fraction increases and particle size decreases.
- Particle volume fraction decreases as flow rate decreases and falling length increases.
- Large-scale particle receiver with long falling height undergoes significant volume fraction decrease due to accelerated particle velocity.
- Part load operation of a particle receiver and long falling height enhances heat loss by solar energy transmission through the particle curtain.
- The transmission loss problem will get worse if a particle receiver is designed for larger temperature differences with smaller flow rates.
- Uneven temperature distribution across the falling particle curtain is likely to be high and it becomes more significant as the absorptivity of particle curtain increases.
- Efficiency of a falling particle receiver in full load operation is estimated to be near 90 %.
- Initially-scoped multiple cavity receiver concept for ASTRI reference field showed 6.6~11.3 % spillage and about 88 % overall efficiency at solar noon on equinox.

ACKNOWLEDGEMENTS

This research was performed as part of the Australian Solar Thermal Research Initiative (ASTRI), a project supported by the Australian Government, through the Australian Renewable Energy Agency (ARENA).

REFERENCES

1. C.K. Ho, J.M. Christian, D. Romano, J. Yellowhair and N. Siegel, Proc. ASME 2015 9th International Conference on Energy Sustainability, San Diego, USA, ES2015-49421.
2. B. Gobereit, L. Amsbeck, R. Buck and C. Singer, ASME 2015 9 th International Conference on Energy Sustainability, San Diego, USA, ES2015-49354.
3. A. Kumar, J.-S. Kim and W. Lipinski, Applied Mathematical Modelling, submitted (2016).
4. K. Ogata, K. Funatsu and Y. Tomita, Powder Technology 115, pp. 90-95 (2001).
5. Tonatiuh, release 2.2.1, http://iat-cener.github.io/tonatiuh/.